Published online July 26, 2006

doi:10.1093/nar/gkl495

Identification of single-point mutations in mycobacterial 16S rRNA sequences by confocal single-molecule fluorescence spectroscopy

Nicole Marmé[1], Achim Friedrich[2], Matthias Müller[3], Oliver Nolte[3], Jürgen Wolfrum[3], Jörg D. Hoheisel[2], Markus Sauer[4] and Jens-Peter Knemeyer[2,*]

[1]Institute of Physical Chemistry, University of Heidelberg, Im Neuenheimer Feld 229, 69120 Heidelberg, Germany, [2]Department of Functional Genome Analysis, German Cancer Research Center, Im Neuenheimer Feld 580, 69120 Heidelberg, Germany, [3]Institute of Physical Chemistry, University of Heidelberg, Im Neuenheimer Feld 253, 69120 Heidelberg, Germany and [4]Applied Laser Physics and Laser Spectroscopy, University of Bielefeld, Universitätsstrasse 25, 33615 Bielefeld, Germany

Received May 22, 2006; Revised June 28, 2006; Accepted June 29, 2006

ABSTRACT

We demonstrate the specific identification of single nucleotide polymorphism (SNP) responsible for rifampicin resistance of *Mycobacterium tuberculosis* applying fluorescently labeled DNA-hairpin structures (smart probes) in combination with single-molecule fluorescence spectroscopy. Smart probes are singly labeled hairpin-shaped oligonucleotides bearing a fluorescent dye at the 5′ end that is quenched by guanosine residues in the complementary stem. Upon hybridization to target sequences, a conformational change occurs, reflected in a strong increase in fluorescence intensity. An excess of unlabeled ('cold') oligonucleotides was used to prevent the formation of secondary structures in the target sequence and thus facilitates hybridization of smart probes. Applying standard ensemble fluorescence spectroscopy we demonstrate the identification of SNPs in PCR amplicons of mycobacterial *rpoB* gene fragments with a detection sensitivity of 10^{-8} M. To increase the detection sensitivity, confocal fluorescence microscopy was used to observe fluorescence bursts of individual smart probes freely diffusing through the detection volume. By measuring burst size, burst duration and fluorescence lifetime for each fluorescence burst the discrimination accuracy between closed and open (hybridized) smart probes could be substantially increased. The developed technique enables the identification of SNPs in 10^{-11} M solutions of PCR amplicons from *M.tuberculosis* in only 100 s.

INTRODUCTION

On a global scale, infectious diseases are the most frequent cause of death. A growing spectrum of so called opportunistic microorganisms and the notorious tendency of microbes to develop resistance patterns against anti-infective drugs (i.e. antibiotics) cause a rapidly growing challenge for routine diagnostic services. A number of methods are available in order to test for antimicrobial susceptibility. The most widely used techniques are culture-based while novel techniques take advantage of specific molecular detection of resistance determinants. Determination of antimicrobial resistance using culture-based methods may be sufficiently fast for rapidly growing microorganisms. However, the discrimination between resistant and wild type slow growers, such as *Mycobacterium tuberculosis*, will benefit remarkably from molecular methods. Rapid, reliable, economic and highly sensitive DNA detection methods have thus become increasingly important in many fields, including health care, environmental studies, physical and biochemical research.

Today, molecular methods already play an important role in early-stage diagnosis of cancer diseases, diagnostic of viral diseases (e.g. HIV infections), laboratory test for the confirmation of tuberculosis and fast detection of antimicrobial resistance mechanisms (1–5). The molecular methods currently available are, however, poorly standardized (many of them being in house methods). Furthermore, sensitivity is still an important issue as these available methods need amplification of the specific target in combination with downstream methods. Consequently, there is a growing interest in diagnostic methods that enable the detection of very small amounts of target DNA.

Current state of the art routine diagnostics constitutes amplification of the target sequence by PCR or related techniques that increase the concentrations of target sequence

*To whom correspondence should be addressed. Tel: +49 622 154 5044; Fax: +49 622 154 5050; Email: knemeyer@single-molecule-spectroscopy.de

The authors wish it to be known that, in their opinion, the first two authors should be regarded as joint First Authors

prior to analysis. The amplified DNA is hybridized to immobilized complementary oligonucleotides and hybridization between target sequence and probe is visualized by use of chromogenic techniques (e.g. GenoType *Mycobacterium* direct kit or the GenoType MTBDR kit, Hain Lifescience, Nehren, Germany). In contrast to heterogeneous assay formats, homogeneous assays enable the detection of specific DNA sequences without washing or separation steps. One approach uses a probe consisting of a short fluorescently labeled oligonucleotide complementary to the target sequence and fluorescence correlation spectroscopy (FCS) to monitor hybridization to the target sequence by an increase in diffusion time or a change in fluorescence polarization (6,7). Other assays are based on two dye-labeled oligonucleotides that form a fluorescence resonance energy transfer (FRET)-pair which disappears upon hybridization of a probe oligonucleotide to the target sequence (8). Generally, single nucleotide polymorphism (SNP) analysis is performed using commercially available template directed dye terminator incorporation (TDI) (9) or the TaqMan assay (10). Alternatively, the ligase detection reaction (LDR) assay can be used for identification of SNPs (11). Here two oligonucleotides that hybridize in direct neighborhood are ligated if they perfectly match the target DNA. Applying ensemble fluorescence spectroscopy these standard methods exhibit detection limits in the micro- to nanomolar range.

Recent methods like the molecular beacons developed by Tyagi and Kramer (12,13) use probes that report the presence of a specific DNA sequence by an increase in fluorescence intensity. These probes are based on hairpin-shaped oligonucleotides labeled with a fluorescent dye and a quenching moiety. The loop sequence of the hairpin probe is complementary to the target DNA. Upon hybridization to the target, fluorescence quenching is reduced owing to the formation of the thermodynamically favored double helix. Molecular beacons can be used for SNP analysis in the nanomolar range under optimized conditions (14). Instead of using organic quencher molecules like DABCYL or the more effective black hole quencher (BHQ) (15), also gold nanoparticles have been successfully applied (16). The major advantage of these types of self-quenched probes is their application in homogeneous DNA assays because they do not require any washing or separation step and they enable online monitoring of hybridization kinetics (17–19).

Recently, an alternative technique for specific detection of target sequences was introduced that takes advantage of the fact that several oxazine and rhodamine derivatives are selectively quenched by the DNA base guanine (20–26). The method uses the low oxidation potential of the DNA base guanine to efficiently quench the fluorescence of suited fluorophores via photoinduced electron transfer upon contact formation (26). These so-called smart probes (22) are relatively easy to design because only a single labeling step is required and they exhibit a free terminus for further modification of the hairpin, e.g. for immobilization on a solid support without further chemical modifications in the loop (Figure 1) (24). With careful design of these conformational flexible DNA probes and the selection of appropriate fluorophores, efficient and highly sensitive DNA-hairpins can be synthesized that increase fluorescence intensity up to 20-fold upon specific hybridization to target sequences (23). Applying

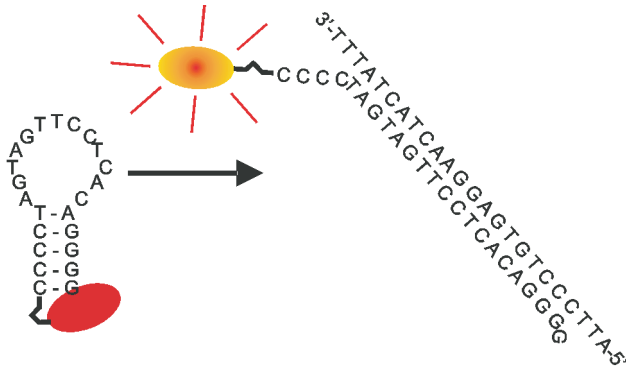

Figure 1. Principle of operation of smart probes. The fluorophore is attached to the 5′ end of the oligonucleotide and quenched by guanosine residues in the complementary stem. Hybridization to the target sequence forces the stem apart and completely restores the fluorescence because efficient quenching of the fluorophore by guanosine residues requires contact formation.

smart probes in time-resolved single molecule fluorescence spectroscopy measurements, we demonstrated a detection limit for synthetic target sequences well below the nanomolar range (22).

In the present work, we demonstrate the identification of SNPs in PCR amplified subgenic fragments of the *rpoB* gene (which codes for the DNA dependent RNA polymerase) of *M.tuberculosis* using smart probes in homogeneous assays. As proof of principle we investigated a mutation that causes rifampicin resistance in *Mycobacteria*. Here, displacement of an adenine by a thymine residue (GAC → GTC) at position nt 1322 of the *rpoB* gene causes an amino acid substitution in the protein sequence and induces rifampicin resistance. The particular mutation chosen is one of the most common ones and serves as model to optimize the described detection technique. Rifampicin resistance may, however, as well be caused by other mutations. The current literature lists ∼90 different mutations, mainly within a short 81 bp fragment of the gene (27–30).

In contrast to the detection of synthetic target sequences using DNA-hairpin probes, the detection of mutations in amplified target samples, i.e. PCR amplicons, is more complicated because of the formation of secondary structures (25). In order to reduce the effect of secondary structures in the target sequence we used an excess of flanking 'cold' oligonucleotides to guarantee the accessibility of the target sequence for hybridization of the smart probe. Applying confocal single-molecule fluorescence spectroscopy in combination with multiparameter analysis we demonstrate the identification of SNP in 10^{-11} M solutions of PCR amplicons from *M.tuberculosis* in only 100 s.

MATERIALS AND METHODS

Synthesis and spectroscopic characteristics of smart probes

All oligonucleotides were purchased from IBA (Göttingen, Germany). For the smart probe-*WT* (wild type) and for the smart probe-*M* (mutant) the oligonucleotides CCC TCT GGT CCA TGA ATT GAG GG and CCC TCT GGA CCA TGA ATT GAG GG were modified at their 5′ end using

C_6-amino-linker. For fluorescence labeling the oligonucleotides were mixed in carbonate buffer (0.1 M, pH 8.5) with a 10-fold excess of the N-hydroxysuccinimidyl ester of ATTO655 (Atto-Tec GmbH, Siegen, Germany). The reaction solution was incubated for 12 h at room temperature before the product was finally purified by HPLC (Hewlett-Packard, Böblingen, Germany) using a reversed-phase column (Knauer, Berlin, Germany) with octadecylsilanehypersil C18. A linear gradient (20 min) from 0 to 75% acetonitrile containing 0.1 M triethylammoniumacetat was used for separation. All fluorescence spectra and temperature profiles were obtained from a Cary Eclipse fluorescence spectrometer (Varian, Darmstadt, Germany) and 50 µl-cuvettes. Absorption spectra were measured on a Cary 500 UV-Vis-NIR spectrometer (Varian, Darmstadt, Germany) using standard quartz cuvettes with an optical pathway of 10 mm. Ensemble fluorescence lifetime measurements were carried out with an IBH spectrometer (model 5000MC, Glasgow, Scotland) using the technique of time-correlated single-photon counting (TCSPC). All measurements were performed at pH 7.0 in phosphate-buffered saline (PBS) containing 140 mM NaCl. To exclude polarization effects, fluorescence was observed under magic angle (54.7°) conditions. Typically, 5000 photon counts were collected in the maximum channel using 2056 channels. The decay parameters were determined by least-square deconvolution, and their quality was judged by the reduced χ^2 values and the randomness of the weighted residuals. In case that a monoexponential model was inadequate to describe the measured decay, a multiexponential model was used to fit the decay (Equation 1),

$$I(t) = I(0) \sum a_i \tau_i, \qquad \mathbf{1}$$

where a_i are the pre-exponential factors that describe the ratio of the excited species and τ_i denote their lifetimes.

Preparation of the PCR-products

PCR was carried out applying standard protocols. Briefly, primers Tr8 (TGCACGTCGCGGACCTCCA) and Tr9 (TCGCCGCGATCAAGGAGT) were used in a concentration of 5 pmol/µl in final reaction volumes of 100 µl. DNA poylmerase and PCR reagents were obtained from MBI Fermentas (St Leon Rot, Germany). The thermal cycling profile consisted of 95°C (denaturation for 60 s), 57°C (primer annealing for 60 s) and 72°C (extension for 60 s). PCR products were checked for the expected length in 2% agarose gels. Purified amplicons were used for cycle sequencing applying standard protocols where reagents were obtained from Applied Biotech, Mörfelden, Germany. Sequence analysis was done on an ABI Prism 310 analyzer. Only amplicons with verified sequence (i.e. absence or presence of the resistance conferring mutation) were used for hybridization experiments. Secondary structures of the PCR amplicons were calculated using *mfold* (31). The program uses nearest-neighbor energy rules to estimate the free energies of possible secondary structures of a given DNA sequence.

Hybridization of smart probes to target DNA amplicons

For ensemble measurements the respective smart probe was mixed in PBS (pH 7.0) containing 140 mM NaCl with a 10-fold excess of target DNA (artificial oligonucleotides or PCR amplicons) resulting in a final concentration of the smart probe of 1×10^{-8} M whereas the concentration of the target DNA was 1×10^{-7} M. Before addition of the PCR amplicons it was denaturated for 10 min at 97°C and chilled on ice. The mixed solutions were heated to 65°C and slowly cooled down to 25°C with a gradient of 0.4°C per minute. Samples were prepared in the same way for single-molecule experiments, but the concentration of the smart probes was 5×10^{-10} M. The samples were transferred onto a microscope slide with a small depression and covered by a cover slide.

Single molecule spectroscopy data analysis

The experimental setup for single-molecule measurements is based on a standard inverse fluorescence microscope (Axiovert 100TV, Zeiss, Germany) and is described in more detail elsewhere (22,32). Briefly, a pulsed diode laser emitting light at 635 nm with a repetition rate of 80 MHz and a pulse duration of <100 ps full width at half-maximum (PDL800B, Picoquant, Berlin, Germany) served as an excitation source. Passing an excitation filter (639DF9, Omega Optics, Brattleboro, VT) the collimated laser beam was coupled into an oil-immersion objective (100×, NA = 1.4, Nikon, Japan) by a dichroic beam splitter (645DMLP; Omega Optics, Brattleboro, VT). The average laser power was adjusted to 600 µW at the sample. Fluorescence light was collected with the same objective and focused through the TV outlet of the microscope onto a 100 µm pinhole. Fluorescence light passing through the pinhole was filtered by a longpass filter (650 nm) and focused onto the active area of an avalanche photodiode (AQR-14, EG&G, Canada). The detector signal was registered by a PC plug-in card for time-correlated single-photon counting (TCSPC) (SPC-630, Becker&Hickl, Berlin, Germany). The photons recorded on the TCSPC card were summed into 1 ms time bins to generate multi-channel-scalar (MCS) traces (Figure 2). To analyze the MCS-traces, a peak recognition filter (Burst scout, Atto-Tec, Siegen, Germany) extracting bursts that have a maximum intensity above a certain threshold was applied. We used a burst recognition threshold of 30 kHz (Figure 2, black line). For each burst >30 MHz, the burst duration (in milliseconds), maximum intensity, overall intensity (total number of photons) and the fluorescence lifetime were calculated and stored. To determine the fluorescence lifetime (decay time) of each burst, the arrival times of all photons of the respective burst were histogrammed with respect to the laser pulse (Figure 2, inset). Fluorescence lifetimes were calculated using a maximum likelihood estimator (MLE) algorithm (33,34).

For FCS measurements the APD output was connected to a correlator card (model 5000/E, ALV, Langen, Germany). Six runs of 30 s were averaged to get a correlation curve. All fluorescence signals were measured at room temperature (25°C). Fluorescence intensity autocorrelation functions were calculated by the correlator board and saved as ASCII files. The autocorrelation functions were analyzed with Origin (Microcal Software, Northhampton, MA). FCS measures the fluorescence fluctuations arising from fluorescent molecules as they pass the detection volume to obtain information about dynamic processes at the molecular level (35). Using FCS,

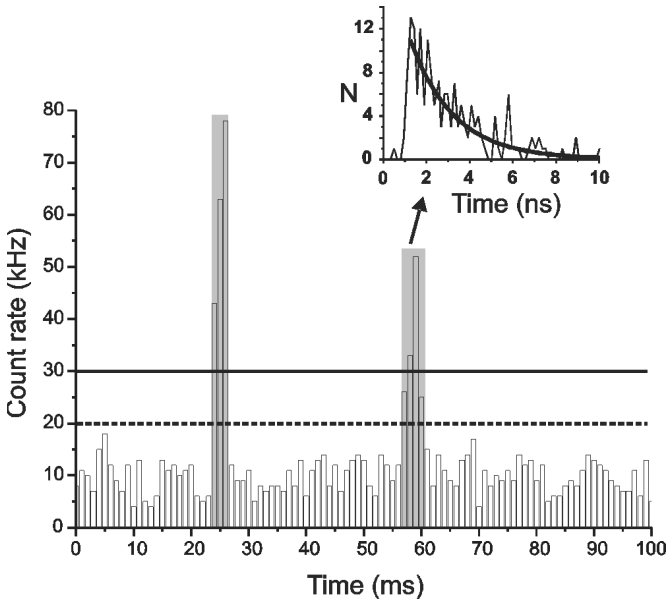

Figure 2. Fluorescence intensity with time (MCS-trace) recorded from a 5×10^{-10} M solution of a smart probe (1 ms/bin). Fluorescence bursts are defined by a recognition threshold, i.e. a count rate of 30 kHz (black line). Origin and end of a burst were defined by a count rate of 20 kHz (dashed line). The fluorescence lifetimes of recognized bursts were calculated applying a MLE-algorithm. Using the described burst recognition definition, we identify two fluorescence bursts at ~25 ms (223 photon counts, 3 ms burst duration, fluorescence lifetime, $\tau = 2.9$ ns) and at ~58 ms (138 photon counts, 4 ms burst duration, fluorescence lifetime, $\tau = 2.2$ ns).

the time dependent fluorescence signal $F = \delta F + \langle F \rangle$ is described by the fluorescence fluctuations $\delta F(t)$ about an average value $\langle F \rangle$. These fluctuations are analyzed in the form of a normalized autocorrelation function $G(\tau)$, where τ denotes the correlation time (Equation 2).

$$G(\tau) = \frac{\langle F(t)F(t+\tau)\rangle}{\langle F(t)\rangle^2} = 1 + \frac{\langle \delta F(t)\delta F(t+\tau)\rangle}{\langle F(t)\rangle^2} \qquad \mathbf{2}$$

FCS can be used to gain information about all processes influencing the fluorescence intensity in the detection volume, e.g. translational diffusion, triplet states or equilibrium constants (35–37).

RESULTS

Spectroscopic characteristics of smart probes

Owing to the small number of compounds with intrinsic fluorescence >600 nm, near-infrared (NIR) fluorescence detection in bioanalytical samples is a desirable alternative to visible fluorescence detection (38–40). This fact, as well as the availability of diode laser for this spectral region, has prompted our efforts to develop so-called smart probes (Figure 1) based on NIR dyes (20–22). For our experiments, we synthesized two smart probes using the red-absorbing dye ATTO655. In aqueous solvents, ATTO655 exhibits an absorption maximum at 661 nm, and emits at an emission maximum of 673 nm with a fluorescence lifetime τ of 1.85 ns. The smart probe ATTO655-*WT* contains a DNA sequence complementary to the wild-type PCR product whereas the smart probe ATTO655-*M* fits the mutant PCR product. Both probes, ATTO655-*WT* and ATTO655-*M*, show bathochromic shifts of a few nanometers in the absorption and emission spectra in aqueous solvents compared to spectra of the free fluorophore, indicating the formation of non- or only weakly fluorescent complexes. Upon addition of an excess synthetic target sequence (short complementary oligonucleotides) to smart probes, spontaneous hybridization occurs, reflected in an ~7-fold increase in fluorescence intensity. The fluorescence decays of the closed smart probes ATTO655-*WT* and ATTO655-*M* could be best described using a biexponential model with $\tau_1 = 2.71 \pm 0.34$ ns ($a_1 = 0.76 \pm 0.06$), $\tau_2 = 0.42 \pm 0.18$ ns ($a_2 = 0.24 \pm 0.08$). Accordingly, we measured an increase in fluorescence lifetime upon addition of an excess of target sequence. The fluorescence decays measured after hybridization show an almost monoexponential decay with $\tau_1 = 2.93 \pm 0.25$ ns ($a_1 = 0.98 \pm 0.04$), $\tau_2 = 0.32 \pm 0.16$ ns ($a_2 = 0.02 \pm 0.02$). Comparison of the changes in fluorescence intensity and lifetime before and after hybridization to artificial target sequences shows that quenching electron transfer reactions between guanosine residues and ATTO655 are mainly manifested by static quenching. This indicates that the quenching reaction is faster than the time resolution of our TCSPC apparatus of ~40 ps. (27)

Influence of the secondary structure of the PCR amplicon on hybridization efficiency

Although the double-stranded PCR product was denatured for 10 min at 97°C and immediately chilled on ice, addition of a 10-fold excess of single-stranded PCR product did not result in a significant increase in fluorescence intensity in contrast to the addition of short artificial target DNA oligonucleotides. This can be attributed to the formation of suboptimal secondary structures of the PCR product (25). As depicted in Figure 3. the calculated secondary structure for the 157 bp PCR amplicon of *M.tuberculosis* is not accessible for hybridization of a smart probe under the used standard conditions (aqueous buffer containing 140 mM NaCl, 25°C). In particular, 8 of the 15 DNA bases responsible for hybridization of the smart probe (marked dark gray in Figure 3) are involved in base pairing and thus are not accessible for hybridization. Modification of the conditions for secondary structure calculation, e.g. by increasing temperature and varying salt concentration, demonstrates that below a temperature of ~50–60°C several target DNA bases are always involved in double helix formation. To realize hybridization of the smart probes to the PCR product so-called 'cold' or 'breaking' oligonucleotides were used. Such artificial oligonucleotides can rip the secondary structure of the PCR product and therefore facilitate hybridization of the smart probe. In Figure 3 the binding sites for the 'cold' oligonuleotides 1–6 are marked light gray (58–73: cold oligonucleotide 1; 74–98: cold oligonucleotide 2; 99–133: cold oligonucleotide 3; 134–157: cold oligonucleotide 4; 1–19: cold oligonucleotide 5; 20–40; cold oligonucleotide 6). To investigate the influence of cold oligonucleotides on hybridization efficiency, the denaturated PCR product (10^{-7} M) was mixed with the smart probe-*WT* (10^{-8} M) in the presence of different cold

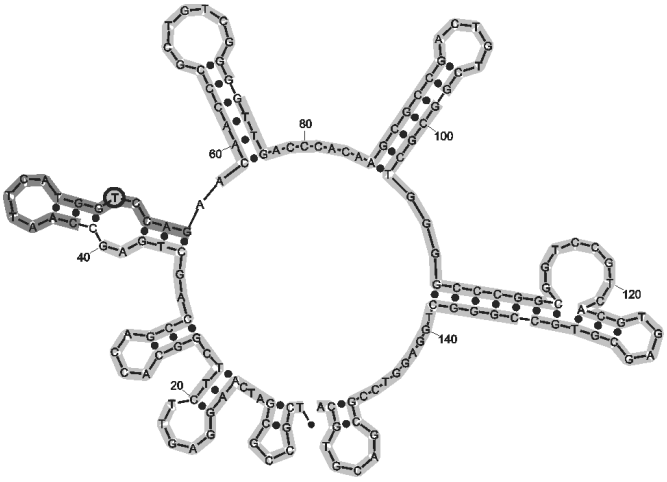

Figure 3. *mfold* structures (modeling parameters: 140 mM Na^+, 0 mM Mg^{2+}, 25°C) of the 157 bp PCR amplicon of *M.tuberculosis*. The binding sites for the loop sequence of the smart probe marked dark gray. The binding sites for the 'cold' oligonuleotides 1–6 are marked light gray (58–73: cold oligonucleotides 1; 74–98: cold oligonucleotides 2; 99–133: cold oligonucleotides 3; 134–157: cold oligonucleotides 4; 1–19: cold oligonucleotides 5; 20–40: cold oligonucleotides 6).

oligonucleotides. Afterwards, the mixture was heated to 65°C and cooled down to 25°C during 100 min. Addition of cold oligonucleotide 1 results in a 1.4-fold increase in fluorescence intensity whereas all other cold oligonucleotides (1–5) generate a smaller increase in the range of 1.1–1.2 fold. Upon simultaneous addition of all cold oligonucleotides 1–6, a 2.0-fold increase in fluorescence intensity was measured. In addition, the influence of various combinations of cold oligonucleotides was studied (data not shown). In conclusion the results demonstrate that addition of cold oligonucleotide 1 is most effective in breaking the secondary structure of the PCR product. However, in order to achieve the best results addition of all six cold oligonucleotides is advantageous.

Applying this technique and the two smart probes (smart probe-*WT* and smart probe-*M*), discrimination between the wild-type amplicon and the mutant amplicon containing the SNP was easily possible. In these experiments, the mixture containing the matching or non-matching smart probe together with the denaturated PCR products and all cold oligonucleotides was heated to 65°C and subsequently cooled down very slowly (0.05°C per minute) before ensemble fluorescence measurements. Using conventional fluorescence spectroscopy, we achieved an increase in fluorescence intensity of up to 2-fold in the presence of relative large amounts of complementary target PCR-products ($\sim 10^{-6}$ M) with a detection limit in the 10^{-8} M range. Even though limited in sensitivity, the introduced assay technique exhibits great potential when applied in combination with time-resolved single-molecule fluorescence spectroscopy.

Time-resolved single-molecule fluorescence spectroscopy

Single-molecule fluorescence spectroscopy (SMFS) enables the investigation of characteristics of individual molecules, i.e. identification of subpopulations in a heterogeneous

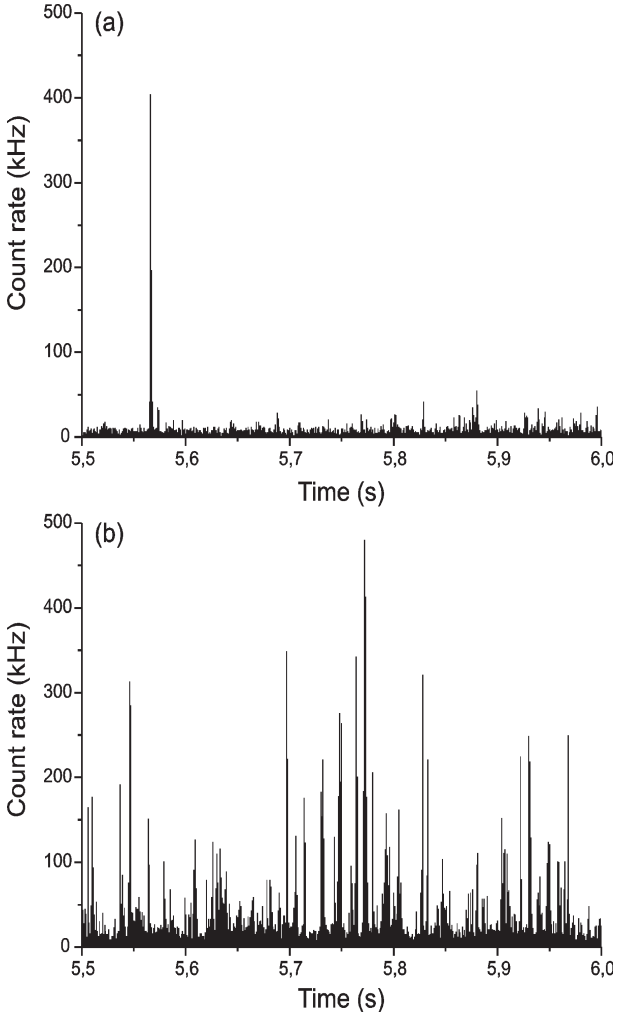

Figure 4. Fluorescence intensity (MCS)-traces observed from a 5×10^{-10} M solution of smart probe-*M* before and after addition of a 100-fold excess of an artificial target DNA. Measurements were carried out at room temperature in PBS (pH 7.0) containing 140 mM NaCl at an average excitation power of 0.6 mW at the sample.

mixture, while ensemble measurements yield only information on average properties (41). Figure 4 shows the fluorescence intensities recorded over time (MCS-traces) of a 5×10^{-10} M solution of smart probe-*M* in the absence and presence of a perfectly matching artificial target DNA. The average count rate measured for smart probe-*M* of ~12.5 kHz increases to ~45 kHz after addition of an excess of artificial target sequence. Considering a background signal of ~7.5 kHz measured for pure buffer, we estimate, in accordance with ensemble measurements, a 7–8-fold increase in overall fluorescence intensity upon hybridization to the perfectly matching artificial target sequence. However, as compared to ensemble spectroscopy, SMFS might be advantageously used in diagnostic applications because it enables an improved discrimination between closed (quenched smart probes), and probes that are hybridized to target DNA. The reason for the improved discrimination stems from the fact that fluorescence signals of fluorophores can be easily separated from background signal that also contains Raman and Rayleigh scattering, as well as autofluorescence

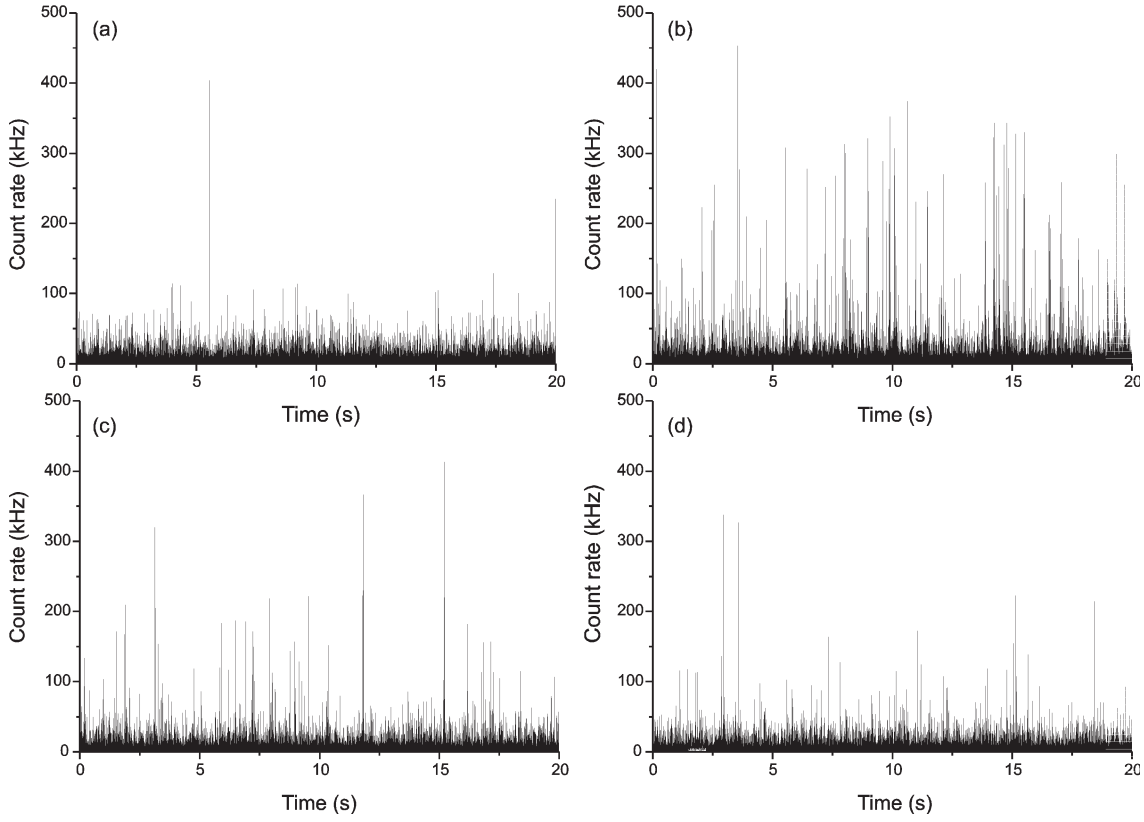

Figure 5. Fluorescence intensity traces observed from 5×10^{-10} M solution of the smart probe-*M* in absence (**a**) and presence of (**b**) 2×10^{-8} M, (**c**) 1×10^{-9} M and (**d**) 5×10^{-11} M of the matching PCR-product. To all samples the cold oligonucleotides 1–6 were added. Before measuring all samples were heated to 65°C and cooled down to 25°C over night. Measurements were carried out at room temperature in PBS (pH 7.0) containing 140 mM NaCl using an average excitation power of 0.6 mW.

of impurities. Therefore, signals with higher count rates (>30 kHz) corresponding to smart probes diffusing through the detection volume can be easily extracted from the monitored MCS-trace. The closed smart probes show almost only signals <100 kHz in the absence of target DNA. Only very few signals, i.e. <1%, show higher count rates that could be somehow caused by opened probes, probes in which the fluorophores do not interact with a guanosine residue in the complementary stem, or by free fluorescent dyes that might still be present even after HPLC purification.

On the other hand, after adding an excess of artificial target DNA, fluorescence bursts with maximum count rates between 100 and 600 kHz are evident (Figure 4b). During a measurement time of 100 s, we found 7616 fluorescence bursts for the hybridized and 63 fluorescence bursts for the closed (unbound) smart probe, respectively, with a count rate >100 kHz. Thus, the number of fluorescence signals above the selected threshold of 100 kHz increases by a factor of ~121, i.e. much stronger than determined in ensemble fluorescence experiments. In standard cuvette experiments we found an ~7-fold increase in fluorescence intensity upon addition of an excess of complementary target sequence. To further increase the discrimination efficiency between open and closed smart probes, we determined simultaneously the fluorescence decay time for each burst recognized above the 100 kHz threshold. As expected from ensemble measurements the fluorescence decay time of smart probes increases considerably upon addition of target sequence. Applying a monoexponential MLE-algorithm results in a typical fluorescence decay time of ~1.2 and ~3 ns for the closed and open smart probe, respectively (22).

The major aim of this work was the highly sensitive and specific identification of a SNP responsible for rifampin resistance in *M.tuberculosis*. Therefore, different concentrations of the PCR-products of the wild type and the mutant form were mixed in PBS with smart probe-*WT* and smart probe-*M* (containing a single mismatch in the loop sequence), respectively. Furthermore, all six cold oligonucleotides were added in order to avoid secondary structures. Finally, the solutions were heated and slowly cooled down from 65 to 25°C during 14 h before experiments were performed with a typical measurement time of 100 s. Figure 5 shows 20 s sections of the raw data recorded from four different samples of the mutant smart probe-*M* in the presence of different concentrations of the corresponding PCR-product. The MCS-trace of the pure smart probe-*M* shows mainly fluorescence bursts with a maximum count rate well below 100 kHz (Figure 5a). Only few signals with higher count rates can be observed. Upon addition of a 40-fold excess (2×10^{-8} M) of the matching PCR product the fluorescence signal increases as can be seen by the increasing number of fluorescence bursts with count rates >100 kHz (Figure 5b).

In agreement with ensemble measurements the increase in fluorescence intensity upon hybridization of smart probes to

real samples, i.e. to PCR products, is less pronounced. Using background corrected average count rates we calculate only a 2-fold increase in fluorescence intensity upon addition of a 40-fold excess of matching PCR product in the presence of all cold oligonucleotides. In the presence of lower concentrations of matching PCR product the average increase in count rate is even less pronounced. However, the fluorescence intensity traces shown in Figure 5c and d clearly demonstrate the potential of SMFS. Even in the presence of only 5×10^{-11} M of matching PCR product the MCS-trace reveals slightly higher fluorescence bursts than without addition of any PCR product (compare Figure 5a and d). In contrast, the addition of a 40-fold excess of the respective non-matching PCR product to smart probe-*WT* or smart probe-*M* neither results in an increased average count rate nor in an increase in the number of fluorescence bursts with count rates >100 kHz (data not shown). In order to quantify the concentration of target sequence present in the sample we compared the spectroscopic properties of the fluorescence bursts of the closed smart probes and probes that are hybridized to the PCR product (Figure 6). The signals were obtained from MCS-traces as shown in Figure 5a and b.

First, we investigated the intensity of the fluorescence signals, which is the sum of all photons detected per fluorescence burst (Figure 6a). The burst size, i.e. the number of photon counts detected per burst, increases significantly after hybridization to the target PCR-product. Less than 1% of the closed smart probes show intensities >220 photons/burst. In contrast, for the probes hybridized to the matching PCR-product over 12% of the signals exhibit a burst size of >220 photons/burst. Above 150 photons/burst, the hybridized probe shows significantly more signals (22.2%) than the pure smart probe (4.0%). Furthermore, the fluorescence lifetime changes owing to hybridization (Figure 6b). For the closed hairpin probe the fluorescence signals show fluorescence lifetimes centered around 1 ns, corresponding to ensemble lifetime data measured for closed smart probes. For <6% of the signals detected for closed probes, fluorescence lifetimes longer than 2.25 ns were measured. After adding an excess of artificial target DNA we found a Gaussian-shaped lifetime distribution centered at 2.8 ns and <10% of the signals below 2.25 ns (data not shown). On the other hand, addition of a 40-fold excess of matching PCR-product does not induce the hybridization, i.e. opening, of all hairpin probes. Here, we found a bimodal lifetime distribution with two maxima at ~1.3 ns and ~2.5 ns. Nevertheless, fluorescence decay time information (Figure 6b) is suited as additional parameter to increase the identification accuracy of opened (unquenched) smart probes. More than 34% of the signals show a fluorescence life longer than 2.25 ns. Upon hybridization to the PCR-product not only an enhancement of the fluorescence intensity and lifetime is observed, but also the burst duration time enhances, i.e. the diffusion constant increases because of the increase in molecular weight (Figure 6c). In the experiments presented, a 23 nt containing smart probe hybridizes to a 157 nt containing PCR product including several cold oligonucleotides. Thus, the molecular weight increases considerably. While 99.5% of all unhybridized probes show diffusion times shorter than 5 ms, 10% of the hybridized hairpins exhibit diffusion times longer than 5 ms (Figure 6c). Already at a burst duration of 4 ms we found

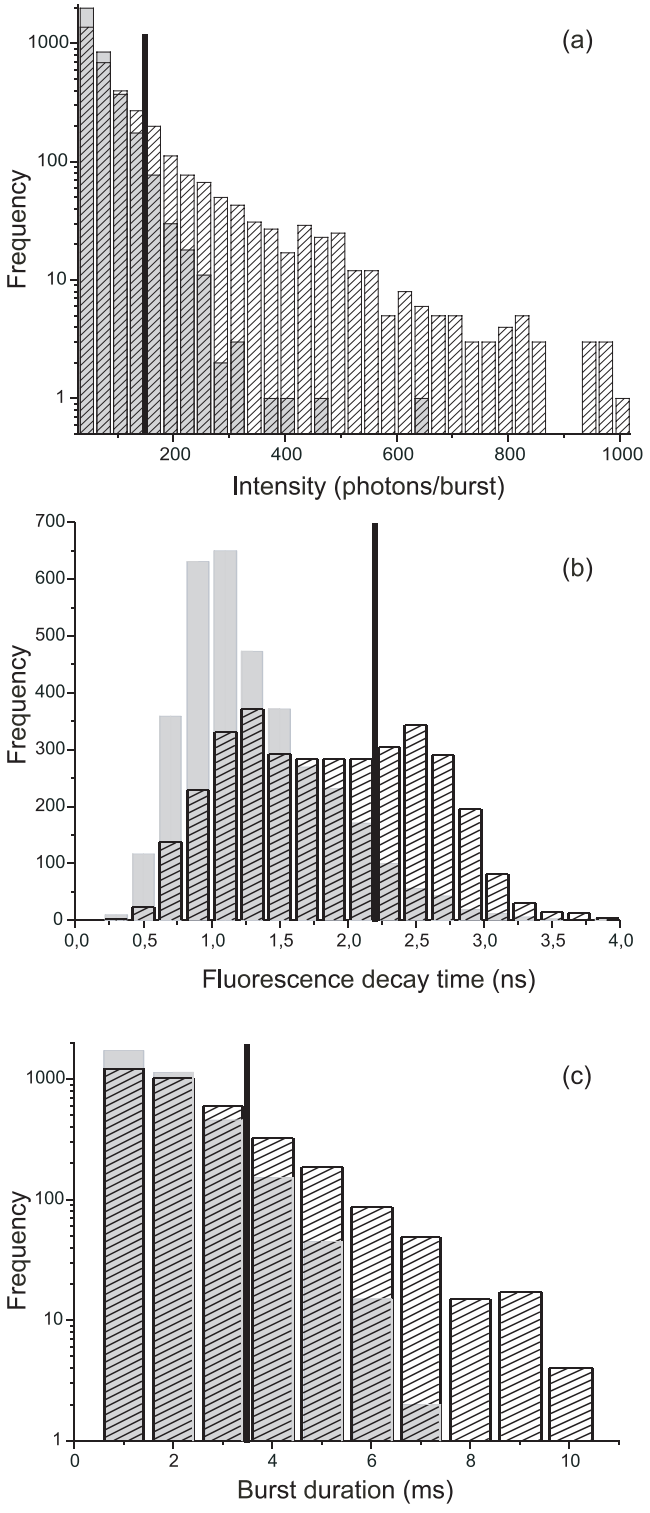

Figure 6. (**a**) Burst size, (**b**) fluorescence decay time and (**c**) burst duration distribution of 3500 photon bursts detected from a 5×10^{-10} M solution of smart probe-*M* in the absence (gray) and presence (open) of 2×10^{-8} M matching PCR product.

significantly more signals for the hybridized probe (19.3%) than for the unhybridized probe (6.1%).

Figure 6a and c clearly demonstrate that the combination of all three parameters can substantially increase the

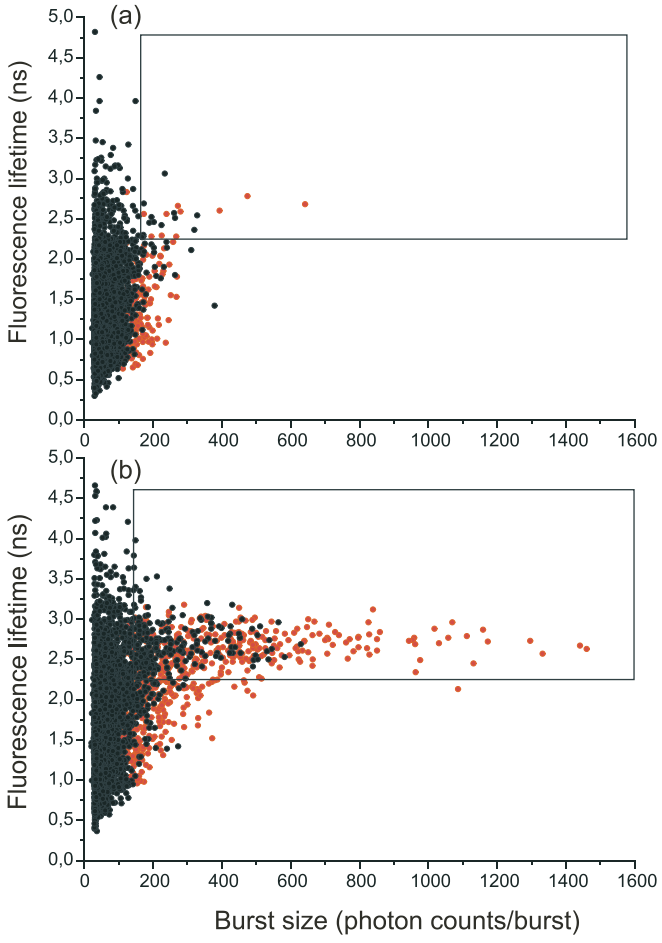

Figure 7. Fluorescence lifetime of each signal measured from a 5×10^{-10} M solution of the smart probe-*M* (**a**) in the absence and (**b**) presence of 2×10^{-8} M of the matching PCR-product is plotted versus the respective burst size (photon counts/burst). Signals with a burst duration ⩾4 ms are marked red.

identification accuracy of hybridized smart probes. Therefore, we plotted the burst size versus the fluorescence lifetime for each signal measured in the absence and presence of matching PCR-product (Figure 7). Furthermore, all signals with burst durations of four or more milliseconds were color encoded in red. Comparison of the two scatter plots clearly uncovers an area defined by the rectangle in Figure 7 where mainly signals from hybridized smart probes are located. During a measurement time of 100 s smart probe-*M* shows only 10 fluorescence signals (i.e. 0.2% of all signals recorded) with a lifetime >2.25 ns, a burst size >150 photon counts and a burst duration of longer than 4 ms in the absence of matching PCR-product (red circles in Figure 7a). In contrast, in the presence of 2×10^{-8} M matching PCR-product ~500 fluorescence signals (i.e. ~10% of all signal) are located within the same area (Figure 7b).

Figure 8 shows the number of fluorescence signals located within the area defined in Figure 7 at different PCR-product concentrations of the wild type and mutant form. In the nanomolar range, 5–10 times more signals were found for the smart probe hybridized to the fully matching PCR-product compared to the respective PCR-product containing

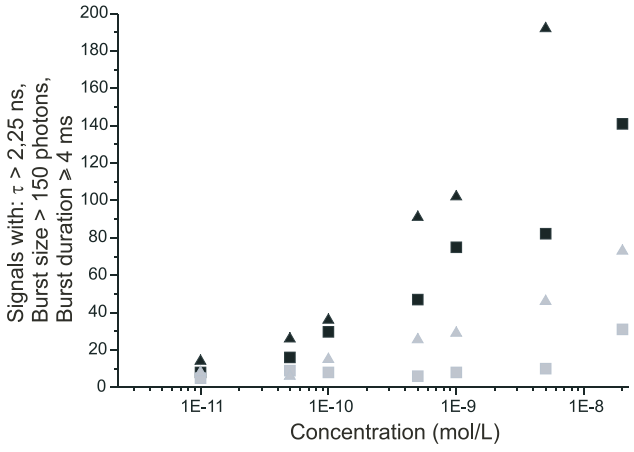

Figure 8. Detected signals of the smart probe-*M* (triangles) and the smart probe-*WT* (squares) with a burst size of >150 photons, a fluorescence lifetime of >2.25 ns and a burst duration of ⩾4 ms during a measurement time of 100 s plotted versus the concentration of PCR-product of the wild type and the mutant of *M.tuberculosis*, respectively. The data points obtained from the matching PCR-product are black and the respective reference sample containing the other PCR-product containing one mismatch is marked gray.

one mismatch. Also for lower concentrations a significant increase in the number of signals located within the area is apparent, e.g. for a concentration of 5×10^{-11} M ~20 signals were found, i.e. a 2-fold increase.

DISCUSSION

In this article we present for the first time the detection of SNP in PCR-products using smart probes. Our study demonstrates that PCR-products show significantly different properties than artificial target-DNA sequences. After addition of a 40-fold excess of a short (20mer) artificial target-DNA to smart probes (5×10^{-9} M) the hairpin-structured probe hybridizes immediately reflected in a 7-fold increase in fluorescence intensity. On the other hand, addition of the same amount of PCR-product has no effect owing to the presence of stronger secondary structures. As shown, the formation of stable secondary structures can be at least partly avoided by adding an excess of unlabeled ('cold') oligonucleotides. Applying this method we observed a 2-fold increase in fluorescence intensity upon addition of an excess of PCR-product.

However, the discrepancy in fluorescence signals between closed and opened smart probes can be further increased by applying single-molecule fluorescence spectroscopy. Owing to the relatively high mass of the DNA-strand including the hybridized 'cold' oligonucleotides, the diffusion time of the fluorescence labeled smart probe decreases significantly upon binding to its target. This effect can be investigated by FCS that analyses the fluctuations of the fluorescence signal. Figure 9a shows FCS measurements of a 5×10^{-9} M solution of smart probe-*WT* in the absence of any target (dotted line), in presence of a 20-fold excess of artificial target DNA (dashed line) and of an excess of matching PCR-product (solid line). The calculated diffusion time for the unhybridized smart probe is ~100 μs and increases to

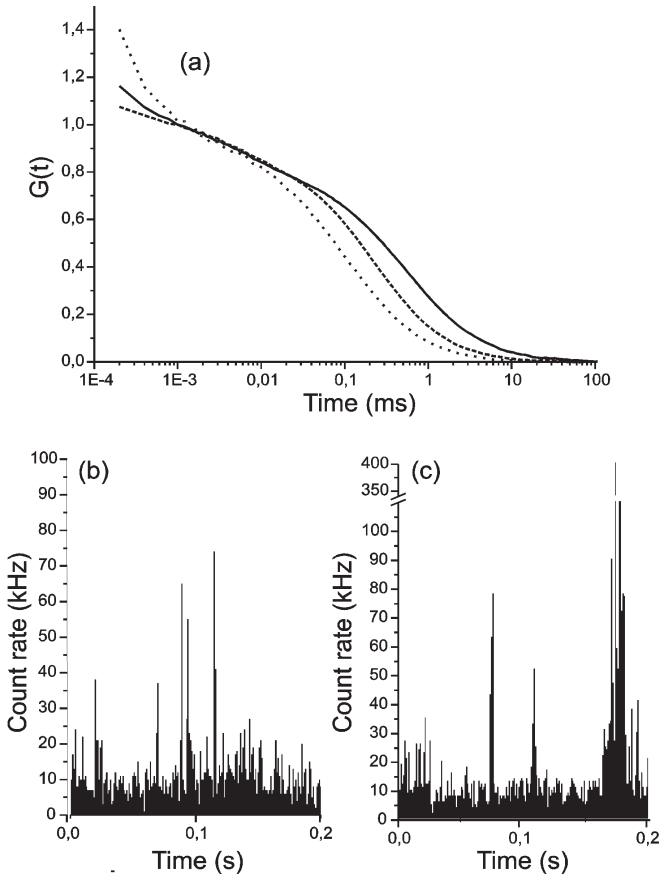

Figure 9. (**a**) FCS measurements of a 5×10^{-9} M solution of the smart probe before (dotted line) and after addition of the artificial target DNA (dashed line) and target PCR-product (solid line), respectively. Furthermore, 200 ms cut-outs of the MCS-traces of a 5×10^{-10} M smart probe sample in the absence (**b**) and the presence (**c**) of the target PCR product.

~180 μs upon addition of artificial target-DNA. Hybridization to the PCR-product results in a diffusion time of ~380 μs which is almost four times longer than the diffusion time of the unhybridized smart probe. Consequently, the analysis of burst durations can help to discriminate between hybridized and unhybridized smart probes. Furthermore, longer diffusion times result in higher burst sizes.

Using standard ensemble fluorescence spectroscopy, smart probe concentrations down to about 10^{-8} M can be measured. However, in the presence of an equimolar amount of PCR-product no significant increase in fluorescence intensity occurs. Even a 40-fold excess of PCR-product is able to open ~15% of the hairpin probes and thus the fluorescence intensity is doubled. A 100% opening of the smart probe generates a 7-fold increase and can be achieved by adding artificial target-DNA. To improve the hybridization of the probe to the target-DNA the hairpin probe could be designed less stable, e.g. by using shorter stems that contain only four base pairs, or one could choose a longer loop sequence that is complementary to the target-DNA. Actually, both ways would result in more efficient hybridization, but on the other hand, this also reduces the specificity of the probes and the quenching efficiency in the closed state. However, the presented smart probes are appropriate to identify a single point mutation in a 157 bp PCR-product of *M.tuberculosis*. We demonstrated that the sensitivity can be enhanced dramatically using single-molecule detection techniques. Measuring the diffusion of individual molecules through the open volume element of a confocal fluorescence microscope presents an easy and fast detection and identification scheme for PCR target sequences in the nanomolar range simply by counting fluorescence signals above a threshold count rate of 150 kHz. At lower concentrations the use of additional information like burst duration, fluorescence lifetime and burst size further improve the discrimination accuracy. To summarize, the proof of principle that smart probes can be utilized for the identification of PCR-targets with single-nucleotide accuracy has been demonstrated. A single point mutation in a PCR-product at very low concentrations down to 10^{-11} M can be detected by time-resolved single-molecule spectroscopy. It has to be investigated in future experiments whether this novel method can be applied for analyzing a broad range of clinical relevant PCR products.

ACKNOWLEDGEMENTS

This work was financially supported by the Bundesministerium für Bildung und Forschung (Grants 13N8349 and 13N8348) and the Landesstiftung Baden-Württemberg and the European Commission as part of the MolTools project. Funding to pay the Open Access publication charges for this article was provided by the German Cancer Research Center.

Conflict of interest statement. None declared.

REFERENCES

1. Telenti,A., Imboden,P., Marchesi,F., Lowrie,D., Cole,S., Colston,M.J., Matter,L., Schopfer,K. and Bodmer,T. (1993) Detection of Rifampicin-resistance mutations in *Mycobacterium tuberculosis*. *Lancet*, **341**, 647–650.
2. Watterson,S.A., Wilson,S.M., Yates,M.D. and Drobiniewski,F.A. (1998) Comparison of three molecular assays for rapid detection of Rifampin resistence in *Mycobacterium tuberculosis*. *J. Clin. Microbiol*., **36**, 1969–1973.
3. Mokrousov,I., Otten,T., Vyazovaya,A., Limeschenko,E., Filipenko,M.L., Sola,C., Rastogi,N., Steklova,L., Vyshnevskiy,B. and Narvskaya,O. (2003) PCR-based methodology for detecting Multidrug-resistant strains of *Mycobacterium tuberculosis* Beijing Family circulating in Russia. *Eur. J. Clin. Microbiol. Infect. Dis*., **22**, 342–348.
4. Carvalho,W.S., Spindola de Miranda,S., Costa,K.M., Araujo,J.G., Augusto,C.J., Pesquero,J.B., Pesquero,J.L. and Gomes,M.A. (2003) Low-stringency single-specific-primer PCR as a tool for detection of mutations in the rpoB gene of rifampin-resistant *Mycobacterium tuberculosis*. *J. Clin. Microbiol*., **41**, 3384–3386.
5. Iwamoto,T. and Sonobe,T. (2004) Peptide nucleic acid-mediated competitive PCR clamping for detection of rifampin-resistant *Mycobacterium tuberculosis*. *Antimicrob. Agents. Chemother*., **48**, 4023–4026.
6. Gibson,N.J., Gillard,H.L., Whitcombe,D., Ferrie,R.M., Newton,C.R. and Little,S. (1997) A homogeneous method for genotyping with fluorescence polarization. *Clin. Chem*., **43**, 1336–1341.
7. Kinjo,M. and Rigler,R. (1995) Ultrasensitive hybridization analysis using fluorescence correlation spectroscopy. *Nucleic Acid Res*., **23**, 1795–1799.
8. Morrison,L.E., Halder,T.C. and Stols,L.M. (1989) Solution-phase detection of polynucleotides using interacting fluorescent labels and competitive hybridization. *Anal. Biochem*., **183**, 231–244.
9. Chen,X. and Kwok,P.Y. (1997) Template-directed dye-terminator incorporation (TDI) assay: a homogeneous DNA diagnostic method

based on fluorescence resonance energy transfer. *Nucleic Acids Res*., **25**, 137–353.
10. Holland,P.M., Abramson,R.D., Watson,R. and Gelfand,D.H. (1991) Detection of specific polymerase chain reaction product by utilizing the 5′→3′ exonuclease activity of *Thermus aquaticus* DNA polymerase. *Proc. Natl Acad. Sci. USA*, **88**, 7276–7280.
11. Chen,X., Livak,K.J. and Kwok,P.Y. (1998) A homogeneous, ligase-mediated DNA diagnostic test. *Genome Res*., **8**, 549–556.
12. Tyagi,S. and Kramer,F.R. (1996) Molecular beacons: probes that fluoresce upon hybridization. *Nat. Biotechnol*., **14**, 303–308.
13. Bonnet,G., Tyagi,S., Libchaber,A. and Kramer,F.R. (1999) Thermodynamic basis of the enhanced specificity of structured DNA probes. *Proc. Natl Acad. Sci. USA*, **96**, 6171–6176.
14. Tyagi,S., Bratu,D.P. and Kramer,F.R. (1998) Multicolor molecular beacons for allele discrimination. *Nature Biotech*., **16**, 49–53.
15. Yao,G. and Tan,W. (2004) Molecular-beacon-based array for sensitive DNA analysis. *Anal. Biochem*., **331**, 216–223.
16. Dubertret,B., Calame,M. and Libchaber,A.J. (2001) Single-mismatch detection using gold-quenched fluorescent oligonucleotides. *Nat. Biotechnol*., **19**, 365–370.
17. Liu,X. and Tan,W. (1999) A fiber-optic evanescent wave DNA biosensor based on novel molecular beacons. *Anal. Chem*., **71**, 5054–5059.
18. Steemers,F.J., Ferguson,J.A. and Walt,D.R. (2000) Screening unlabeled DNA targets with randomly ordered fiber-optic gene arrays. *Nat. Biotechnol*., **18**, 91–95.
19. Culha,M., Stokes,D.L., Griffin,G.D. and Vo-Dinh,T. (2004) Application of a miniature biochip using the molecular beacon probe in breast cancer gene BRCA1 detection. *Biosens. Bioelectron*., **19**, 1007–1012.
20. Sauer,M., Han,K.-T., Müller,R., Nord,S., Schulz,A., Seeger,S., Wolfrum,J., Arden-Jacob,J., Deltau,G., Marx,N.J. *et al*. (1995) New fluorescent dyes in the red region for biodiagnostics. *J. Fluoresc*., **5**, 247–261.
21. Sauer,M., Drexhage,K.H., Lieberwirth,U., Müller,R., Nord,S. and Zander,C. (1998) Dynamics of the electron transfer reaction between an oxazine dye and DNA oligonucleotides monitored on the single-molecule level. *Chem. Phys. Lett*., **284**, 153–163.
22. Knemeyer,J.P., Marmé,N. and Sauer,M. (2000) Probes for detection of specific DNA sequences at the single-molecule level. *Anal. Chem*., **72**, 3717–24.
23. Heinlein,T., Knemeyer,J.P., Piestert,O. and Sauer,M. (2003) Photoinduced electron transfer between fluorescent dyes and guanosine residues in DNA-hairpins. *J. Phys. Chem. B*, **107**, 7957–7964.
24. Piestert,O., Barsch,H., Buschmann,V., Heinlein,T., Knemeyer,J.P., Weston,K.D. and Sauer,M. (2003) A single-molecule sensitive DNA hairpin system based on intramolecular electron transfer. *Nano Lett*., **3**, 979–982.
25. Stoehr,K., Haefner,B., Nolte,O., Wolfrum,J., Sauer,M. and Herten,D.P. (2005) Species-specific identification of mycobacterial 16S rRNA PCR amplicons using smart probes. *Anal. Chem*., **77**, 7195–7203.
26. Kim,J., Doose,S., Neuweiler,H. and Sauer,M. (2006) The initial step of DNA hairpin folding: a kinetic analysis using fluorescence correlation spectroscopy. *Nucleic Acids Res*., **34**, 2516–2527.
27. Heep,M., Brandstatter,B., Rieger,U., Lehn,N., Richter,E., Rusch-Gerdes,S. and Niemann,S. (2000) Frequency of rpoB Mutations Inside and Outside the Clusters I Region in Rifampicin-Resistant Isolates. *J. Clin. Microbiology*, **39**, 107–113.
28. Ramaswamy,S. and Musser,J.M. (1998) Molecular genetic basis of antimicrobial agent resistance in *Mycobacterium tuberculosis*. *Tuber. Lung Dis*., **79**, 3–29.
29. Hwang,H.Y., Chang,C.Y., Chang,L.L., Chang,S.F., Chang,Y.H. and Chen,Y.J. (2003) Characterization of rifampicin-resistant *Mycobacterium tuberculosis* in Taiwan. *J. Med. Microbiol*., **52**, 239–245.
30. Yang,B., Koga,H., Ohno,H., Ogawa,K., Fukuda,M., Hirakata,Y., Maesaki,S., Tomono,K., Tashiro,T. and Kohno,S. (1998) Relationsship between anitmycobacterial activities of rifampicin, rifabutin and KRM-16748 and rpoB mutations of *Mycobacterium tuberculosis*. *Journal of Antimicrobial Chemotherapy*, **42**, 621–628.
31. Zuker,M., Mathews,D.H. and Turner,D.H. (1999) In Barciszewski,J. and Clark,B.F.C. (eds), *RNA Biochemistry and Biotechnology*. NATO ASI Series, Kluwer Academic Publishers, Dordrecht, pp. 11–43(http://bioweb.pasteur.fr/seqanal/interfaces/mfold.html).
32. Tinnefeld,P., Herten,D.P. and Sauer,M. (2001) Photophysical dynamics of single dye molecules studied by spectrally-resolved fluorescence lifetime imaging microscopy (SFLIM). *J. Phys. Chem. A*, **105**, 7989–8003.
33. Tellinghuisen,J. and Wilkerson,C.W.,Jr (1993) Bias and precision in the estimation of exponential decay parameters from sparse data. *Anal. Chem*., **65**, 1240–1246.
34. Soper,S.A. and Legendre,B.L.,Jr (1994) Error analysis of simple algorithms for determining fluorescence lifetimes in ultradilute dye solutions. *Appl. Spectrosc*., **48**, 400–405.
35. Magde,D., Elson,E.L. and Webb,W.W. (1972) Thermodynamic fluctuations in a reacting system—measurement by fluorescence correlation spectroscopy. *Phys. Rev. Lett*., **29**, 705–708.
36. Widengren,J. and Schwille,P. (2000) Characterization of photoinduced isomerization and back-isomerization of the cyanine dye Cy5 by fluorescence correlation spectroscopy. *J. Phys. Chem. A*, **104**, 6416–6428.
37. Widengren,J., Schweinberger,E., Berger,S. and Seidel,C.A.M. (2001) Two new concepts to measure fluorescence resonance energy transfer via fluorescence correlation spectroscopy: theory and experimental realizations. *J. Phys. Chem. A*, **105**, 6851–6866.
38. Aubin,J.E. (1979) Autofluorescence of viable cultured mammalian cells. *J. Histochem. Cytochem*., **27**, 35–43.
39. Affleck,R.L., Ambrose,W.P., Demas,J.N., Goodwin,P.M., Schecker,J.A., Wu,M. and Keller,R.A. (1996) Reduction of luminescent background in ultrasensitive fluorescence detection by photobleaching. *Anal. Chem*., **68**, 2270–2276.
40. Sauer,M., Zander,C., Müller,R., Ullrich,B., Drexhage,K.H., Kaul,S. and Wolfrum,J. (1997) Detection and identification of individual antigen molecules in human serum with pulsed semiconductor lasers. *Appl. Phys. B*., **65**, 427–431.
41. Tinnefeld,P. and Sauer,M. (2005) Branching out of single-molecule fluorescence spectroscopy: challenges for chemistry and influence on biology. *Angew. Chem. Int. Ed*., **44**, 2642–2671.